Soft Matter

PAPER

Cite this: *Soft Matter*, 2018, **14**, 7680

Meniscus instabilities in thin elastic layers

John S. Biggins [a] and L. Mahadevan *[bc]

Received 19th May 2018,
Accepted 30th August 2018

DOI: 10.1039/c8sm01033a

rsc.li/soft-matter-journal

We consider meniscus instabilities in thin elastic layers perfectly adhered to, and confined between, much stiffer bodies. When the free boundary associated with the meniscus of the elastic layer recedes into the layer, for example by pulling the stiffer bodies apart or injecting air between them, then the meniscus will eventually undergo a purely elastic instability in which fingers of air invade the layer. Here we show that the form of this instability is identical in a range of different loading conditions, provided only that the thickness of the meniscus, a, is small compared to the in-plane dimensions and to two emergent in-plane length scales that arise if the substrate is soft or if the layer is compressible. In all such situations, we predict that the instability will occur when the meniscus has receded by approximately $1.27a$, and that the instability will have wavelength $\lambda \approx 2.75a$. We illustrate this by also calculating the threshold for fingering in a thin wedge of elastic material bonded to two rigid plates that are pried apart, and the threshold for fingering when a flexible plate is peeled from an elastic layer that glues the plate to a rigid substrate.

1 Introduction

Interfacial instabilities are commonly associated with fluid–fluid interfaces. The most celebrated examples are Saffman–Taylor fingering[1] when a less viscous fluid invades a more viscous one in a porous media, Rayleigh–Taylor fingering[2,3] when a dense fluid invades a lighter one under the influence of gravity, and the Rayleigh–Plateau instability where a column of fluid breaks into droplets under the influence of its surface tension.[4] More recently, there has been growing interest in analogs of these fluid instabilities in soft solids, including direct observations of Rayleigh–Taylor fingers in soft solid slabs[5] and surface tension driven instabilities in soft solid cylinders.[6–8] Here we focus on a range of recent observations of fingering in soft solids.[9,10] These instabilities typically occur in thin elastic layers adhered to rigid bodies that arise naturally whenever a soft polymeric glue is used, or when a rubber gasket forms a seal.[11]

The viscous analogue of this instability, Saffman–Taylor fingering has long been explored, experimentally and theoretically, by confining a viscous fluid between two glass plates (a Hele Shaw cell) then injecting a less viscous fluid into it.[12] It is found that the less viscous fluid invades the more viscous fluid *via* radial finger-like protrusions, with a wavelength set by a competition between capillary and viscous stresses. Many previous studies have examined how the morphology of fluid Saffman–Taylor fingers changes when the fluid properties are changed. These included studies of fingering involving high viscosity contrast and low interfacial tension fluids that yield thin fractally branching fingers,[13,14] associated with a transition from fingering to fracture,[15–22] and similar patterns in yield stress and shear thinning fluids,[15,23–26] and chemically reactive interfaces.[27–29]

The soft-solid analogue of this experiment consists of pumping air into a cavity in a strongly confined thin elastic layer.[9] At first the cavity simply dilated, but, at a critical pressure, the uniformly circular meniscus gives way to fingers of air that invaded the solid layer. Identical fingers have also been seen in elastic layers trapped between rigid bodies if the air is induced to invade the solid layer by pulling the bodies apart while maintaining adhesion.[10,30] In both cases the fingering transition has been observed to be reversible, rate-independent and subcritical, in sharp contrast with the viscous analogs where the fingering instability is irreversible, rate dependent and supercritical.

This class of interfacial instabilities in confined solids is one of four different elastic instabilities have been identified in elastic layers in tension. Three of these arise when an elastic layer adhered between rigid bodies is pulled apart whilst maintaining adhesion. This leads to one of the following: cavitation in the bulk of the elastic layer,[31] fingering at the meniscus of the elastic layer[10,30] or an undulating fringe instability localized around the contact line between the layer's meniscus and the rigid body.[32,33] The fourth tensile instability

[a] *Department of Engineering, University of Cambridge, Trumpington St., Cambridge CB2 1PZ, UK. E-mail: jsb56@cam.ac.uk*
[b] *School of Engineering and Applied Sciences, and Departments of Organismic and Evolutionary Biology, and Physics, Harvard University, Cambridge, Massachusetts, 02138, USA. E-mail: lmahadev@g.harvard.edu*
[c] *Kavli Institute for Nanobio Science and Technology, Harvard University, Cambridge, Massachusetts, 02138, USA*

is entirely different: when adhesion between the layer and the body fails, 2-D patterns of adhered and de-adhered regions emerge on the previously adhered elasticity.[34–40] Which of these instabilities occurs first depends on the aspect ratio of the elastic layer. Cavitation occurs in very thin layers, fingering in layers of intermediate thickness, and fringing in layers that have an in-plane dimension comparable to their thickness.[41] Here we show that the key driver for fingering is inward displacement of the layer's meniscus, which can be achieved by pulling apart on the rigid bodies, but also arises *via* direct fluid invasion. Thus, unlike fringing and cavitation, meniscus fingering is not an inherently tensile instability, but rather an invasive instability.

Previously theoretical frameworks for understanding the elastic fingering transition[10] are based on two approximations: (i) the displacements in the elastic layer vary quadratically through its thickness, and (ii) the deformations of the elastic layer preserve its depth averaged volume. These approximations allow us to model the three-dimensional layer with an effective two-dimensional elastic theory to predict the onset and wavelength of the fingering instability in a minimal rectilinear setting.[10] Generalizing this framework to annuluar geometries predicted elastic fingering on the inner circumference when the plates are pulled apart or when air is pumped into the central cavity, establishing the equivalence of these two superficially different modes of fingering.[42] Here, we seek to move beyond the very specific geometries treated previously and investigate the generality of fingering in elastic meniscii.

We first consider elastic fingering in a thin layer, with in-plane dimensions much larger than its thickness. We show that if the meniscus of the elastic layer recedes into the layer then it will eventually become susceptible to fingering, and that both the threshold degree of recession and the wavelength of the fingers depend only on the thickness of the layer, not on any other factors pertaining to the morphology of the layer or the loading of the rigid bodies. This shows that the form of the elastic fingering transition is relatively generic.

We illustrate this by considering fingering during the opening a thin elastic wedge and peeling a glued plate from a rigid substrate. Using our general results for the onset of fingering and the resulting instability wavelength, we deploy them in these specific geometries to calculate the degree of loading required for the meniscus of the elastic layer to retreat sufficiently and trigger fingering. The wedge problem is of interest because it offers an alternative perspective on a very old problem[43,44] moving our focus from the tip of a loaded elastic wedge to the thick end where fingering first occurs. The peeling problem is noteworthy because we do not treat the substrate as rigid, allowing us to ask how stiff the rigid body needs to be for fingering to occur. We show the bending of the plates introduces a new in-plane length scale, $a^{1/2}(\kappa/\mu)^{1/6}$, where κ is the plate bending modulus, μ the layer's elastic modulus and a its thickness, which quantifies the length-scale over which the plate bends. Fingering follows the universal form provided this length-scale is much larger than the thickness a.

In the final sections we consider the effects of finite bulk modulus and surface tension on elastic fingering, showing that the former introduces a second in-plane length, $a\sqrt{B/\mu}$, which must also be large compared to a for fingering to follow the universal form, while the latter introduces an elasto-capillary length γ/μ which must be short compared to a for surface tension to remain negligible. Our study concludes by pointing out that elastic fingering has a universal form in layers that are thin compared to their in-plane length scales, including $a\sqrt{B/\mu}$ and $a^{1/2}(\kappa/\mu)^{1/6}$, but thick compared to γ/μ. Given the latter scale is typically measured in microns, elastic fingering will have the same form in a wide range of layers of intermediate thickness.

2 Mechanics of meniscus fingering in thin layers

We consider a thin elastic layer that might have a varying thickness, and a complex in-plane shape with curved boundaries, confined between stiff but not necessarily completely rigid bodies. We assume that the layer is thin in the sense that all the length scales, $\{l_i\}$, that characterize the geometry of the layer (for example the layer's in-plane width, the radii of curvature of its boundaries and the length scales over which the thickness changes and over which the rigid bodies flex) are large compared to the thickness of the layer. We then focus our attention on a region at the meniscus of the elastic layer that is large compared to its thickness, a, but small compared to all the other length-scales. This smallness means that our region has essentially constant thickness and an essentially straight boundary. This allows us to construct a locally rectilinear coordinate system so that the elastic layer occupies the region $-a/2 < z < a/2, y > 0$ as shown in Fig. 1.

When air is induced to invade the elastic layer by either pressurizing it so that it is physically forced to invade the layer, or by prying apart the stiff bodies which increases the volume between them and sucks air in, the meniscus is forced to deform. In either case we assume adhesion is maintained between the elastic layer and the stiff-bodies, so that the meniscus takes the form sketched on the right of Fig. 1. If the inward displacement of the central plane of the elastic layer at the boundary is u, the strain at the boundary scales as u/a. The meniscus loses stability and invaginates when this strain is of order unity,[10] which is when these non-linearities become important. An immediate consequence of this observation is that we expect any separation of the stiff bodies to be much less than the thickness of the elastic layer. To see this, we note that if the rigid bodies separate by an amount Δa the change in volume between them is ΔaA, where A is the in-plane area of the layer. For soft elastic layers that are almost incompressible, this must equal the volume of air sucked in, which we can estimate as uac where c is the length of the meniscus of the layer. Putting these two results together, we conclude that $\Delta a \sim a^2c/A \ll a$ at threshold, so that in the limit of a very thin layer, the required separation becomes vanishingly small.

To go beyond this scaling result, we start with a description of the elastic deformation of the layer by the three-dimensional

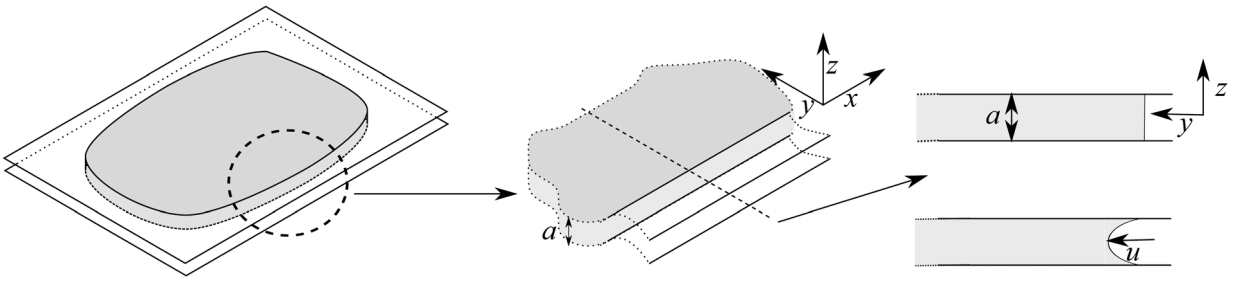

Fig. 1 Sketch of a highly elastic layer (shown in grey) between and adhered to two stiff bodies. We consider a very general case in which the shape of the layer may be any shape, the thickness of the layer may vary and the stiff bodies may bend rather than being completely rigid, but we assume that all of these forms of variation occur over distances much larger than the layer thickness. We concentrate on a section of the boundary, magnified in the middle, which is large compared to the thickness of the layer but small compared to all these other length-scales of variation. In this region the elastic layer has constant thickness a and a single straight meniscus. We set up an x–y–z coordinate system on the boundary as shown in the sketch such that the undeformed elastic layer occupied the region $-a/2 < z < a/2, y > 0$. Finally, on the right, we sketch a 2-D slice of this magnified region (at constant x). The top figure shows the undeformed layer confined between the stiff bodies. The bottom figure shows the layer after air has been drawn in (for example by very slightly separating the bodies) showing how air invades the layer whilst perfect adhesion is maintained between the layer and the stiff bodies. The displacement u measures how far the meniscus of the layer has retreated.

displacement field $\mathbf{U}(x,y,z)$. Focusing our attention on the meniscus region sketched in Fig. 1, we note that the displacement of the rigid bodies is very small compared to a, and so we neglect it as a first approximation. Perfect adhesion between the stiff bodies and the layer then requires $\mathbf{U}(x,y,\pm a/2) = 0$. Since this boundary region also has a constant thickness it is symmetric around the $z = 0$ plane. We exploit the thinness and symmetry of the meniscus region to expand out its displacement field to second order in z as

$$\mathbf{U}(x,y,z) = (1 - 4z^2/a^2)\mathbf{u}(x,y) \tag{2.1}$$

where $\mathbf{u}$ is the two dimensional in-plane displacement of a point on the central ($z = 0$) plane. Using ∇ as the two dimensional (in the x–y plane) gradient operator and I as the two dimensional identity tensor, we can then write the deformation gradient tensor $F_{ij} = \delta_{ij} + \partial_j \mathbf{U}_i$ as

$$F = I + (1 - 4z^2/a^2)\nabla\mathbf{u} - 8z\mathbf{u}\hat{\mathbf{z}}/a^2 + \hat{\mathbf{z}}\hat{\mathbf{z}}. \tag{2.2}$$

We model the elastic layer as an incompressible neo-Hookean material with an elastic energy density given by $\frac{1}{2}(\mathrm{Tr}(F \cdot F^T) - 3)$. This energy density can be explicitly integrated in the thickness (z) direction to give an effective two-dimensional elastic energy, while enforcing incompressibility in terms of a two dimensional pressure field $P(x,y)$ as a Lagrange multiplier which constrains the thickness averaged volume at each point in the x–y plane. The two-dimensional energy density of the elastic layer is then given by

$$L[\mathbf{u}, P] = \mu\int_{-a/2}^{a/2} \frac{1}{2}\left(\mathrm{Tr}\left(F \cdot F^T\right) - 3\right) - P(\mathrm{Det}(F) - 1)\mathrm{d}z \tag{2.3}$$

$$= \frac{5\mu a}{6}\left(\frac{1}{2}\mathrm{Tr}\left(G \cdot G^T\right) - 2 + \frac{16}{5}|\mathbf{u}/a|^2 - P(\mathrm{Det}(G) - 1)\right) \tag{2.4}$$

where we have introduced an effective two dimensional deformation gradient $G = I + \frac{4}{5}\nabla\mathbf{u}$. We see that the effective two dimensional energy density consists of a standard two-dimensional elastic energy and a term that penalizes displacement directly (rather than gradients of displacement), which captures the fact that displacing the central plane of the layer strains the layer adhered to the boundary at $z = \pm a/2$. We now seek to minimize this energy, so we find the Euler–Lagrange equations for the two fields $\mathbf{u}$ and P:

$$\frac{4}{5}a^2\nabla^2\mathbf{u} - \mathrm{Det}(G)G^{-T} \cdot a^2\nabla P = 8\mathbf{u} \tag{2.5}$$

$$\mathrm{Det}(G) = 1. \tag{2.6}$$

These Euler–Lagrange equations are augmented by the following natural boundary condition (given by $\partial L/\partial\nabla\mathbf{u}\cdot\hat{n} = 0$ on the boundary)

$$(G - P\,\mathrm{Det}(G)G^{-T})_{y=0}\cdot\hat{\mathbf{y}} = 0. \tag{2.7}$$

We next consider the deformation of the elastic layer prior to fingering. This base state is characterized by $\mathbf{u}$ varying over the long length scales associated with the in-plane geometry of the layer but not on length scales comparable to the thickness of the layer. We therefore Taylor-expand $\mathbf{u}$ on the boundary to get

$$\begin{aligned}\mathbf{u}(x,y) = &\left(c_1 + c_2\frac{x}{l_1} + c_3\frac{y}{l_2} + c_4\frac{x^2}{l_3^2} + \ldots\right)\hat{\mathbf{x}} \\ &+ \left(d_1 + d_2\frac{x}{l_4} + d_3\frac{y}{l_5} + d_4\frac{x^2}{l_6^2} + \ldots\right)\hat{\mathbf{y}},\end{aligned} \tag{2.8}$$

where the $\{l_i\}$ are in-plane lengths with $l_i \gg a$. Since the region of the meniscus we are focussing on is small compared to all the in-plane lengths, only the zeroth order term in this series is relevant, giving

$$\mathbf{u}(x,y) = c_1\hat{\mathbf{x}} + d_1\hat{\mathbf{y}}. \tag{2.9}$$

With this very simple form for $\mathbf{u}$ we see that $G = I$, *i.e.* eqn (2.6) is already satisfied. Solving eqn (2.5) for P we get

$$P = P_0 - \frac{8c_1x}{a^2} - \frac{8d_1y}{a^2}, \tag{2.10}$$

where P_0 is a constant of integration. We substitute these results into the boundary condition, eqn (2.7), to get

$$1 - P_0 + \frac{8c_1 x}{a^2} = 0, \tag{2.11}$$

from which we conclude that $P_0 = 1$ and $c_1 = 0$, *i.e.* prior to fingering all displacements near the meniscus are perpendicular to it.

The uniform displacement receding displacement of the meniscus d_1 in the base state implies that the term on the right of eqn (2.5) into a spatially homogeneous driving force. The origin of this force is the through-the-thickness quadratic profile of the displacement in the layer. This leads to the stress in the layer varying linearly as one approaches the boundary (eqn (2.10)). We thus see that in general, a sinusoidal perturbation of an interface is associated with a net movement of material along the interface outward normal. There is thus an analogy with the case of a gravitational field acting on an elastic interface, as this will cause a sinusoidal perturbation to release gravitational potential energy so (provided this release outweighs the perturbation's elastic cost) that fingers can grow as in the elastic analog of Rayleigh–Taylor fingers.[5] Correspondingly, in the confined elastic layer case, a sinusoidal perturbation will generate a net movement of the elastic layer back towards its zero displacement, releasing some of the elastic energy associated with the quadratic displacement profile. If this energy release is larger than the shear elastic energy associated with the distortion, the perturbation will grow and the front will be unstable. Elastic fingering is therefore mathematically analogous to Rayleigh–Taylor fingering, although it occurs in physical circumstances reminiscent of Saffman–Taylor fingering.

To determine when fingering becomes favourable, we now consider the stability of the above base state to fingering by adding an infinitesimal short-wave length perturbation to the base state giving

$$\mathbf{u} = (d_1 + \varepsilon f(y)\cos(kx))\hat{\mathbf{y}} + \varepsilon g(y)\sin(kx)\hat{\mathbf{x}} \tag{2.12}$$

$$P = 1 - \frac{8d_1 y}{a^2} + \varepsilon h(y)\cos(kx). \tag{2.13}$$

The effective two-dimensional deformation tensor G is now given by

$$G = \begin{pmatrix} 1 & 0 \\ 0 & 1 \end{pmatrix} + \frac{4}{5}\varepsilon \begin{pmatrix} g(y)k\cos(kx) & g'(y)\sin(kx) \\ -f(y)k\sin(kx) & f'(y)\cos(kx) \end{pmatrix}. \tag{2.14}$$

The first order correction to the volume conservation equation (eqn (2.6)) is simply

$$g(y) = -\frac{f'(y)}{k}. \tag{2.15}$$

Then, the inverse–transpose of the two-dimensional deformation tensor G is given by

$$\mathrm{Det}(G)G^{-T} = \begin{pmatrix} 1 & 0 \\ 0 & 1 \end{pmatrix} + \frac{4}{5}\varepsilon \begin{pmatrix} f'(y)\cos(kx) & f(y)k\sin(kx) \\ -g'(y)\sin(kx) & g(y)k\cos(kx) \end{pmatrix}, \tag{2.16}$$

so it is straightforward to expand out the x component of the bulk Euler–Lagrange equation (eqn (2.5)) to first order in ε to get

$$-\frac{4}{5}a^2k^2g(y) + \frac{4}{5}a^2g''(y) + a^2kh(y) + \frac{4}{5}8f(y)kd_1 = 8g(y), \tag{2.17}$$

which, upon substituting for $g(y)$ using eqn (2.15), can be rearranged to give

$$h(y) = -\frac{4}{5a^2k^2}\left(8d_1k^2f(y) + \left(10 + a^2k^2\right)f'(y) - a^2f'''(y)\right). \tag{2.18}$$

The y component of eqn (2.5) can also be expanded out to first order in ε, giving

$$-\frac{4}{5}a^2k^2f(y) + \frac{4}{5}a^2f''(y) - a^2h'(y) + \frac{4}{5}f'(y)8d_1 = 8f(y), \tag{2.19}$$

which, upon substitution for $h(y)$ and $g(y)$ (from eqn (2.15) and (2.18)) gives the following fourth order equation for $f(y)$:

$$k^2(10 + a^2k^2)f(y) - 2(5 + a^2k^2)f''(y) + a^2f''''(y) = 0, \tag{2.20}$$

subject to stress free boundary conditions (eqn (2.7)) at $y = 0$, and decay conditions at infinity, $f(y \to \infty) \to 0$. We thus initially write f as the sum of the two decaying solutions:

$$f(y) = Ae^{-\frac{\sqrt{10+a^2k^2}y}{a}} + Be^{-ky}. \tag{2.21}$$

To find the constants of integration, (A, B) we expand the stress-free boundary condition, eqn (2.7), to linear order in ε giving

$$\frac{4}{5}\begin{pmatrix} g'(0) \\ f'(0) \end{pmatrix} - \frac{4}{5}\begin{pmatrix} f(0)k \\ g(0)k \end{pmatrix} - \begin{pmatrix} 0 \\ h(0) \end{pmatrix} = \begin{pmatrix} 0 \\ 0 \end{pmatrix}. \tag{2.22}$$

Substituting our results for f, g and h from (2.16), (2.19) and (2.22) into the x component of the boundary conditions yields an algebraic equations for A/B which we can solve to get

$$\frac{A}{B} = -\frac{a^2k^2}{5 + a^2k^2}. \tag{2.23}$$

We can then use the y component of the boundary condition to find the uniform base state of the displacement d_1 in the y direction. Noting that $f'(y) = -kg'(y)$, the equation is equivalent to $8f'(0) = 5h(0)$, or, substituting in for f and h,

$$8 \times Bk\left(\frac{ak\sqrt{a^2k^2 + 10}}{a^2k^2 + 5} - 1\right) = 5 \times \frac{8B}{a}\left(\frac{1}{ak} - \frac{4d_1/a}{a^2k^2 + 5}\right). \tag{2.24}$$

Solving for d_1, the threshold for instability is then:

$$\frac{d_1}{a} = \frac{25 + a^2k^2\left(10 + ak\left(ak - \sqrt{10 + a^2k^2}\right)\right)}{20ak}. \tag{2.25}$$

Finally, to obtain the threshold of the first unstable fingering mode, we minimize the above expression over k to find that the first unstable mode has a wavelength ($\lambda = 2\pi/k$) of

$$\lambda = 2.74601\ldots a \tag{2.26}$$

and occurs at a threshold value of d_1

$$d_1 = 1.26756\ldots a. \tag{2.27}$$

We recall that the coefficient d_1 corresponds to the displacement of points on the boundary of the elastic layer half way between the stiff bodies. The above calculation reveals any mechanism designed to draw air into a thin confined elastic layer will first cause the layer to retract homogeneously normal to the meniscus and then, when the layer has retracted by amount $1.27\ldots a$, fingers of air with a wavelength of $2.74\ldots a$ will protrude into the layer.

These universal geometric conditions for elastic fingering (including wavelength, threshold retraction strain) apply whenever a confined layer retracts, provided only that the layer is thin. This thinness requirement allows both the confinement geometry and base-state retraction to vary in-plane, provided they do so on length-scales long compared to a, the boundary layer thickness.

3 Meniscus fingering induced by opening wedges

To move beyond this general picture to specific situations, we first consider the opening of a thin wedge-shaped elastic layer confined between rigid plates. The initial angle of the elastic wedge is 2α and the layer is perfectly adhered to the two plates as sketched in Fig. 2. Air is then drawn into the layer by opening the angle between the plates to $2(\alpha + \delta\alpha)$. The requirement of layer-thinness here means the wedge angle must be small, $\alpha \ll 1$, so that, for example, the layer thickness varies very little within the finger-forming region at the open end of the wedge. Using an r–θ–z coordinate system (as shown in Fig. 2) the elastic layer initially occupies the region $r < l$, $-\alpha < \theta < \alpha$.

After deformation the point in the elastic layer at (r, θ, z) is moved to $(R(r,\theta,z), \Theta(r,\theta,z), Z(r,\theta,z))$. In a thin wedge θ is the thickness coordinate so we expand out these fields to second order in θ. The symmetry condition $\theta \to -\theta$ implies that $R(r,\pm\alpha,z) = r$, $Z(r,\pm\alpha,z) = z$ and $\Theta(r,\pm\alpha,z) = \pm(\alpha + \delta\alpha)$ to maintain perfect adhesion between the layer and the plates, giving

$$R(r,\theta,z) = r + (1 - (\theta/\alpha)^2)u_r(r,z) \tag{3.28}$$

$$\Theta(r,\theta,z) = \frac{\alpha + \delta\alpha}{\alpha}\theta \tag{3.29}$$

$$Z(r,\theta,z) = z + (1 - (\theta/\alpha)^2)u_z(r,z). \tag{3.30}$$

The general form for the deformation gradient, F, in polar coordinates (after a rigid body rotation that ensures the reference and target points have $\theta = \Theta$) is

$$F = \begin{pmatrix} \frac{\partial R}{\partial r} & \frac{1}{r}\frac{\partial R}{\partial \theta} & \frac{\partial R}{\partial z} \\ R\frac{\partial \Theta}{\partial r} & \frac{R}{r}\frac{\partial \Theta}{\partial \theta} & R\frac{\partial \Theta}{\partial z} \\ \frac{\partial Z}{\partial r} & \frac{1}{r}\frac{\partial R}{\partial \theta} & \frac{\partial Z}{\partial z} \end{pmatrix}. \tag{3.31}$$

We again formulate a two dimensional effective energy for the elastic layer by modeling the layer as a neo-Hookean solid with thickness (θ) averaged volume preservation, leading to the effective energy density

$$L = \mu\int_{-\alpha}^{\alpha}\frac{1}{2}\left(\mathrm{Tr}\left(F\cdot F^T\right) - 3\right) - P(\mathrm{Det}(F) - 1)r\,\mathrm{d}\theta, \tag{3.32}$$

which is directly analogous to eqn (2.3). While it is possible to determine the onset of wavelength of fingering in this system by substituting the quadratically varying fields (eqn (3.28)–(3.30)), evaluating the θ integral to produce a two-dimensional energy, finding the Euler–Lagrange equations and boundary conditions for the new energy and then conducting a stability analysis on these equations. However, in the light of the results in the previous section we see that we only need to treat the "base-state" to see what separation of the plates, $\delta\alpha$, will lead to sufficient retraction of the layer to drive fingering. We therefore restrict our attention to fields that are translationally invariant in the z direction, giving

$$u_r(r,z) = u_r(r) \tag{3.33}$$

$$u_z(r,z) = 0, \tag{3.34}$$

which simplifies F to

$$F = \begin{pmatrix} \left(1 - \frac{\theta^2}{\alpha^2}\right)u_r'(r) + 1 & -\frac{2\theta u_r(r)}{\alpha^2 r} & 0 \\ 0 & \frac{(\alpha+\delta\alpha)}{\alpha}\left(1 + \left(1 - \frac{\theta^2}{\alpha^2}\right)\frac{u_r(r)}{r}\right) & 0 \\ 0 & 0 & 1 \end{pmatrix}. \tag{3.35}$$

Furthermore, the form of the field $u_r(r)$ is completely determined by the constraint that the thickness averaged volume be preserved (which would be the Euler–Lagrange equation given by varying the pressure in the original energy). This constraint

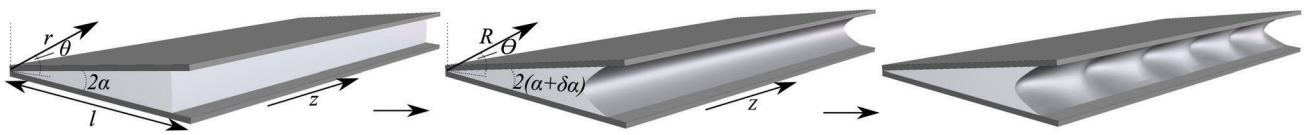

Fig. 2 Sketch of a highly elastic layer (light grey) between and adhered to two rigid plates (dark grey) in a wedge shape. On the left is the unstrained state, labeled with coordinates (r, θ, z), in which the elastic layer occupies the region $-\alpha < \theta < \alpha$ and $r < l$. In the middle is the base deformation state, labeled with coordinates (R, Θ, Z), in which the plates have been opened to make an angle of $2(\alpha + \delta\alpha)$, drawing air into the elastic layer. At a critical value of $\delta\alpha$ fingers of air will protrude into the layer along the $r = l$ boundary, as sketched on the right.

is simply

$$\int_{-\alpha}^{\alpha} (\mathrm{Det}(F) - 1) r \mathrm{d}\theta = 0, \tag{3.36}$$

which, upon substituting the above form for F gives

$$15\delta\alpha r + 2(\alpha + \delta\alpha)((4u_r(r) + 5r)u_r'(r) + 5u_r(r)) = 0. \tag{3.37}$$

This has two solutions for $u_r(r)$ of the form,

$$u_r(r) = \frac{1}{4}\left(-5r \pm \sqrt{\frac{A + 5r^2(5\alpha - \delta\alpha)}{\alpha + \delta\alpha}}\right), \tag{3.38}$$

where A is a constant of integration. Perfect adhesion at the point $r = 0$ requires that $u_r(0) = 0$, which sets $A = 0$. The requirement that if $\delta\alpha = 0$ then there should be no displacement, so $u_r(r) = 0$, requires us to choose the solution

$$u_r(r) = \frac{1}{4} r\left(-5 + \sqrt{-5 + \frac{30\alpha}{\alpha + \delta\alpha}}\right). \tag{3.39}$$

Inspecting the form of the quadratic fields, (eqn (3.28)–(3.30)), we see that $u_r(r)$ represents the displacement in the r direction of a point on the central ($\theta = 0$) plane of the wedge. If the wedge has total length l then the thickness of the wedge at its fat-end is $2\alpha l$. We know from the previous section that the onset of fingering will occur when $u(l) = -1.27\ldots 2\alpha l$, which given us the expression

$$\frac{1}{4}\left(-5 + \sqrt{-5 + \frac{30\alpha}{\alpha + \delta\alpha}}\right) = -1.27\ldots \times 2\alpha. \tag{3.40}$$

If we expand this out for small $\delta\alpha$ we discover that

$$\delta\alpha = 3.38015\ldots\alpha^2. \tag{3.41}$$

Provided the wedge is thin (*i.e.* $\alpha \ll 1$) the expansion is self-consistent. We see, as expected, that the critical degree of opening depends only on the initial angle of the wedge and that, for thin wedges, the required degree of opening to trigger fingering becomes is negligible compared to the thickness of the wedge. We also note that we can also express the wavelength of the instability in terms of the parameters of the wedge as

$$\lambda = 2.74601\ldots \times 2\alpha l = 5.49202\ldots \times \alpha l. \tag{3.42}$$

In thicker wedges, we still expect fingering but it will not follow the universal form. This is so even though the elastic fields associated with the fingers are localized to the open-end of the wedge, they will never-the-less "feel" the diminishing layer thickness and retraction towards the wedge tip. In this case, fingering is expected to morph into a "fringing" form, with separate undulations at the top and bottom plates of the wedge.[32,33]

4 Meniscus fingering induced by peeling

Next we consider a thin elastic layer between a completely rigid substrate and a stiff but somewhat flexible plate that is gently lifted up at one end. This situation is often associated with peeling an adhesive layer with a backing, as sketched in Fig. 3. As in the wedge geometry previously considered, the peeling action increases the volume between the plate and the substrate causing the meniscus of the elastic layer to retreat. This ultimately leads to fingers of air invading the layer at the meniscus. Although the system superficially resembles previous work on peeling plates from soft elastic layers,[35–37,39,40] those studies focussed on the movement of the contact line between layer and plate caused by de-adhesion and were in a linear-elastic regime. In contrast, in the current study, we assume that adhesion is maintained and we operate in the non-linear elastic regime.

Since the plate is not perfectly rigid, we have to understand both its shape as well as that of the meniscus. To model this situation we take our elastic layer to initially occupy the region $0 < z < a, y > 0$ and to be perfectly adhered to a rigid substrate at $z = 0$ and to the plate, which is initially at $z = a$. We then imagine lifting the end of the plate so that the point on the plate initially at (x, y, a) moves to $(x, y, a + h(y))$. Our assumption that the plate only moves in the z direction is justified provided that $h'(y) \ll 1$ since the change to its length caused by this deformation is quadratic in $h'(y)$.

As in our previous examples, we expand the displacement field in the bulk of the elastic layer $\mathbf{U}(x,y,z)$, to leading order in z and impose the condition of perfect adhesion between the layer and the rigid substrate (at $z = 0$) and the plate (at $z = a$) giving:

$$\mathbf{U}(x, y, z) = 4\frac{z(a - z)}{a^2}\mathbf{u}(x, y) + \frac{z}{a}h(y)\hat{\mathbf{z}}, \tag{4.43}$$

where, as in our general treatment, $\mathbf{u}(x,y)$ is a two-dimensional vector in the x–y plane corresponding to the x–y displacement of a point in the elastic layer at $(x, y, a/2)$. We note that the in-plane displacement has a symmetry around $z = a/2$, which is

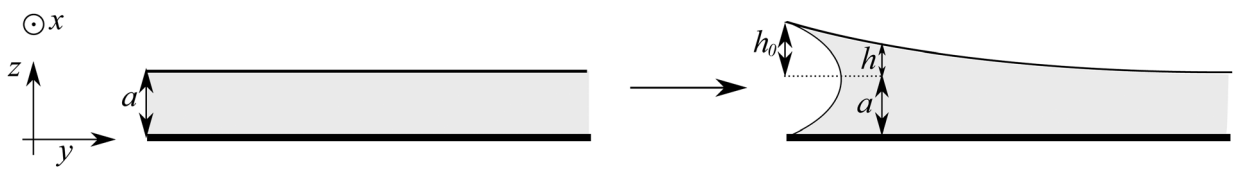

Fig. 3 A thin elastic layer (grey) between a completely rigid substrate (thick black line, bottom) and a stiff (but somewhat flexible) plate (black line, top). On the left is the configuration of plate and layer before any deformation, with the layer occupying the region $y > 0$, $0 < z < a$ and the plate in a flat configuration at $z = a$. On the right is the situation after the ($y = 0$) end of the plate has been lifted by an amount h_0. Consequently the plate at y has lifted by an amount $h(y)$ and air has been drawn into the elastic layer at the $y = 0$ boundary. Fingers of air will eventually invade the layer at this boundary.

perhaps unexpected given the lack of symmetry in this geometry. However, a bit of reflection allows us to see that since any asymmetry arises *via* in-plane variation of h, and this is a higher order effect given that $h'(y) \ll 1$, the observed symmetry is to be expected. This displacement defines a deformation gradient $F = \delta_{ij} + \partial_j \mathbf{U}_i$ which, using ∇ as the in-plate (x–y) gradient operator and I and the in-plane (x–y) identity matrix, we can write as.

$$F = I + \frac{4z(a-z)}{a^2}\nabla\mathbf{u} + \frac{4(2z-a)}{a^2}\mathbf{u}\hat{\mathbf{z}}\hat{\mathbf{z}} + (1 + h/a)\hat{\mathbf{z}}\hat{\mathbf{z}}. \quad (4.44)$$

As in our previous examples, we model the elastic layer as neo-Hookean and add to the elastic energy a two dimensional pressure field $P(x,y)$ to implement the thickness (z) averaged volume preservation. However, in this case our elastic energy for the layer is supplemented by an energetic penalty for bending the plate, which we estimate as $\frac{1}{2}\kappa h''(y)^2$ per unit area of the plate, where κ is the bending modulus of the plate. This leads us to the full two-dimensional effective energy density

$$L = \mu\int_0^a \frac{1}{2}\left(\mathrm{Tr}\left(F\cdot F^T\right) - 3\right) - P(\mathrm{Det}(F) - 1)\mathrm{d}z + \frac{1}{2}\kappa h''(y)^2. \quad (4.45)$$

As with the wedge-case, we can simplify our analysis considerably by restricting attention to the ''base-state'' deformations prior to fingering. In this case we expect translational symmetry (in the x direction) to be maintained, so that

$$P(x,y) = P(y) \quad (4.46)$$

$$\mathbf{u}(x,y) = u_y(y)\hat{\mathbf{y}}. \quad (4.47)$$

Unfortunately, even after focussing on these one-dimensional fields, the resulting Euler–Lagrange equations for L do not admit a closed form solution. However, by assuming that the plate is very much stiffer than the elastic layer, we note that its displacement decays over a length l that is much greater than the thickness of the elastic layer, that is $l \gg a$. This yields a slowly varying in-plane base state, that, as we show, is required for fingering to adopt a universal form. At the instability threshold the displacement of the elastic layer $u_y \sim a$, and further that volume conservation in the elastic layer implies that $hl \sim u_y a$, so that $h \sim u_y \times (a/l) \sim a^2/l$. We therefore rewrite $h(y)$ and $u_y(y)$ as

$$u_y(y) = a\tilde{u}_y(y/l) \quad (4.48)$$

$$h(y) = \frac{a^2}{l}\tilde{h}(y/l), \quad (4.49)$$

where $\tilde{u}_y$ and $\tilde{h}$ are both dimensionless functions of $\mathcal{O}(1)$. Furthermore, since these functions also have rescaled arguments, y/l, at threshold they decay over an interval $y/l \sim 1$, and thus their derivatives are also $\mathcal{O}(1)$. Expanding each term in the energy (4.46) in the small parameter a/l and identifying the leading order terms which dominate when the layer is thin then implies that the first (neo-Hookean) term evaluates to

$$\int_0^a \frac{1}{2}(\mathrm{Tr}\left(F\cdot F^T\right) - 3)\mathrm{d}z = a\left(\frac{8}{3}\tilde{u}_y\left(\frac{y}{l}\right)^2 + \mathcal{O}\left(\frac{a}{l}\right)\right), \quad (4.50)$$

while the constraint term evaluates to

$$\int_0^a (\mathrm{Det}(F) - 1)\mathrm{d}z = a\left(\frac{a}{l}\left(\tilde{h}\left(\frac{y}{l}\right) + \frac{2}{3}\tilde{u}_y'\left(\frac{y}{l}\right)\right) + \mathcal{O}\left(\frac{a^2}{l^2}\right)\right). \quad (4.51)$$

We see that for these terms to be comparable, we expect $P \sim l/a$. Returning to our original variables, we can therefore write the effective energy density, to leading order, as

$$L = \mu a\left(\frac{8u_y(y)^2}{3a^2} - P(y)\left(\frac{h(y)}{a} + \frac{2}{3}u_y'(y)\right)\right) + \frac{1}{2}\kappa h''(y)^2. \quad (4.52)$$

This yields the Euler–Lagrange equations for the three fields, u_y, h and P as:

$$8u_y(y) + a^2P'(y) = 0 \quad (4.53)$$

$$\mu P(y) - \kappa h''''(y) = 0 \quad (4.54)$$

$$3h(y) + 2au_y'(y) = 0. \quad (4.55)$$

and must be augmented by a Dirichlet boundary condition $h(0) = h_0$, consistent with the fact that the end of the plate has been lifted a distance h_0, and $h'(x)$, $h''(x)$, $h'''(x)$ decays far from the meniscus. Minimization of the energy with respect to $u_y(0)$ and $h'(0)$ also leads to the additional natural (Neumann) boundary conditions $\partial L/\partial u_y'|_{y=0} = 0$ and $\partial L/\partial h''|_{y=0} = 0$, so the full set of boundary conditions are:

$$h(0) = h_0, \quad (4.56)$$

$$P(0) = 0, \quad (4.57)$$

$$h''(0) = 0. \quad (4.58)$$

Eliminating $P(y)$ and $u_y(y)$ from the bulk equations, yields a sixth-order linear equation for $h(y)$:

$$\frac{a^3\kappa}{\mu}h^{(6)}(y) - 12h(y) = 0, \quad (4.59)$$

which has solutions which decay with characteristic length $l = (a^3\kappa/\mu)^{1/6}$ as observed in previous studies with a similar geometry.[35] Using this length-scale, and imposing the condition $h(y) \to 0$ as $y \to \infty$, we may write

$$h(y) = c_1\exp\left(-\frac{2^{1/3}3^{1/6}y}{l}\right) + \left(c_2\cos\left(\frac{3^{2/3}y}{2^{2/3}l}\right) + c_3\sin\left(\frac{3^{2/3}y}{2^{2/3}l}\right)\right)\exp\left(-\frac{3^{1/6}y}{2^{2/3}l}\right), \quad (4.60)$$

where c_1, c_2 and c_3 are undetermined constants. Imposing the boundary conditions (eqn (4.56)–(5.58)) on this solution yields

$$c_1 = h_0/3 \quad (4.61)$$

$$c_2 = 2h_0/3 \quad (4.62)$$

$$c_3 = 0, \quad (4.63)$$

and allows us (*via* the remaining Euler–Lagrange equations) to easily determine the full base-state fields $h(y)$, $u_y(y)$, $P(y)$, where the field $u_y(y)$ is the displacement (in the y direction)

of the central $z = a/2$ plane of the elastic layer. The threshold for fingering is, as always, $u_y(0) = 1.27\ldots a$, which then allows us to find the required displacement of the plate

$$h_0 = 1.9179\ldots\frac{a^2}{l} = 1.9179\ldots a^{3/2}\left(\frac{\mu}{\kappa}\right)^{1/6}. \qquad (4.64)$$

We note that the three functions u_y, P, and h are all functions of y/l with the expected magnitude at threshold, where we have identified the long length-scale as $l = \sqrt{a}(\kappa/\mu)^{1/6}$. We also wish to note that although the terms we neglected in L are negligibly small provided $l \gg a$, our linearization of the energy in a/l does not assume the strains in the layer are small; indeed on the contrary, the strains in the layer are of order one at threshold.

5 Role of compressibility and capillarity

Our analysis to date has focused on the case of incompressible elastic materials with an infinite resistance to local volume changes. An infinite bulk-modulus makes the elasticity of a confined layer infinitely long-ranged as a change in volume introduced at one point (for example by injecting air into a cavity) must propagate to the boundary rather than being mitigated by the material around the cavity changing volume. Soft elastomers such as those used in experiments to study these fingering instabilities typically have bulk moduli that are many orders of magnitude larger than their shear modulus, so the assumption of incompressibility is generally an excellent approximation.

Real elastomers are not perfectly incompressible, so that the effects of an imposed volume change decay with a long but finite length-scale. To estimate this long-length scale we consider a thin-strip shaped elastic layer occupying the region $-a/2 < z < a/2$, $-l < y < l$, with $l \gg a$, and adhered to flat rigid plates at $z = \pm a/2$. The flat plates are then separated by an additional distance Δa. If the elastic layer is perfectly incompressible then volume conservation requires that the inward displacement of a point with coordinates y and $z = 0$ be $u \sim \Delta a y/a$, leading to a strain $\gamma \sim u/a \sim \Delta a y/a^2$ and an energy density $\mu(\Delta a y/a^2)^2$. If the layer instead deformed by simply increasing its volume, its fractional volume change would simply be $\Delta a/a$, leading to an energy density $B(\Delta a/a)^2$, where B is the elastomers bulk modulus. Equating these two energy densities, a characteristic in-plane length emerges that scales as $l_2 \sim a\sqrt{B/\mu}$, and is the distance over which the layer behaves in an incompressible way. In the above strip geometry, we expect that if the width of the strip, $l \gg l_2$ then the central portion of the strip will respond to the separation of the plates by increasing its volume, while only the parts of the layer within l_2 of the boundaries will deform in an incompressible way. From the perspective of causing the meniscus of the elastic layer to retreat to drive fingering at the meniscus, the effective width of the strip is therefore reduced to l_2. Then this additional in-plane length scale must be large compared to the thickness of the layer for fingering to proceed along the lines sketched in Section 2.

Real elastic layers also have a finite surface tension γ, requiring us to add a surface energy γA to the elastic energy, where A is the area from the elastic layer's meniscus. The elastic strains associated with finger formation are of order one and are localized to distances of order a of the layer's meniscus, so the change in elastic energy per unit length of boundary is of magnitude $E_{\mathrm{el}} \sim \mu a^2$, while the corresponding surface energy has magnitude $E_{\mathrm{cap}} = \gamma a$. Thus surface tension becomes energetically relevant if $a \leq \gamma/\mu$, the elasto-capillary length. Our surface-tension free theory therefore requires that, in addition to the thickness of the layer being small compared to the previously discussed in-plane length-scales (*i.e.* that the layer be geometrically thin) it must also be thick compared to the elasto-capillary length-scale. Surface tensions in soft materials are typically of magnitude $\gamma \sim 10^{-2}$ J m^{-2} so, even for layers with elastic moduli of $\mu \sim 500$ Pa, the elasto-capillary length is at most a few tens of microns, meaning surface tension will only become relevant in the very thinnest and softest of layers. Our theory ignoring capillary effects thus has a wide range of validity.

6 Conclusions

When an elastic layer that is adhered above and below to rigid bodies has a meniscus that is deformed (either by separating the rigid bodies to suck air in or by injecting air into a cavity in the layer) then, after a threshold, fingers will invade the layer along the meniscus. While previous treatments of this problem have treated specific geometries, here we have considered a broad range of problems that show that the phenomenon is universal, provided that the layer is geometrically thin, *i.e.* all its in-plane length-scales l_i are large compared to the thickness a of the layer. In such situations, the straight meniscus will give way to undulations when forced beyond a threshold, independent of the nature of the forcing. Furthermore, the fingering follows an essentially universal form: the wavelength of the fingers will be the same multiple of the thickness of the layer in all systems, $\lambda \approx 2.74a$, and occurs when the invading air causes the meniscus to retreat by a universal multiple of the thickness of the layer, $u \approx 1.26a$. To treat fingering problems in thin elastic layers, we only need to find the "base-state" deformations (those prior to fingering), and then apply our universal criteria for the onset and wavelength of fingering to this base-state. To illustrate this procedure we calculated the onset of fingering in two geometries: opening an elastic wedge and peeling a stiff plate.

The peeling geometry is reminiscent of an adhesive layer – the thin plate is akin to the backing glued to an elastic layer, and peeling corresponds to de-adhering the plate from a rigid substrate. The instability threshold for peeling before fingering takes place is $h_0 \approx 1.92\ldots a^{3/2}\left(\frac{\mu}{\kappa}\right)^{1/6}$, and thus larger for softer plates. Estimating the bending energy of the plate (per unit length in the x direction) we find $E_{\mathrm{b}} \sim \frac{1}{2}\kappa(h/l_1^2)^2 l_1$, which is of

similar magnitude to the energy of the elastic-layer since l_1 is chosen to minimize the sum of these two contributions. The force required to lift the end of the plate a distance h is $F_h \sim h\kappa/{l_1}^3$, and at the threshold displacement h_0 is $F_{h_0} \sim \kappa^{1/3}\mu^{2/3}$. Thus, although stiffer plates require less displacement to trigger fingering they require more force.

Our conclusion that elastic fingering in these layers has a general form is subject to three important caveats. In addition to the layer being thin in the sense that its in-plane geometric parameters must be large compared to its thickness, there are two ''hidden'' in-plane length-scales that must also be large. The first emerges if the rigid bodies that the layer is trapped between are not perfectly rigid but instead have a large but finite bending modulus κ, and is the length-scale over which the bodies then bend, given by

$$l_1 = \sqrt{a}\left(\frac{\kappa}{\mu}\right)^{1/6}. \tag{6.65}$$

The second ''hidden'' length-scale arises if the elastic layer is not perfectly incompressible but has large bulk modulus B, and is the length-scale over which bulk-deformations become energetically preferable to shear deformations, given by

$$l_2 = a\sqrt{\frac{B}{\mu}}. \tag{6.66}$$

The condition $l_2 \gg a$ is not at all difficult to achieve. For a soft rubber, we can easily have $B/\mu > 10^6$, making $l_2/a \sim 1000$. However, for the very thin layers arising when soft polymeric glues are used, l_2 could easily be rather shorter than the geometric size of the layer, meaning it will be important in determining the separation required to induce fingering. In contrast, $l_1 \gg a$ is a more rigorous constraint. If the elastic modulus of the stiff bodies is μ_p and they have thickness t we expect $\kappa \sim t^3\mu_p$, giving $l_2 \sim \sqrt{at}(\mu_p/\mu)^{1/6}$. The weak dependence on μ_p in this length-scale means that it is very challenging to make this length long by making the rigid bodies out of a stiff material. However, this length-scale can easily be made long by taking thick bodies with large values of t.

The third caveat also relates to a ''hidden'' length scale, the elasto-capillary length

$$l_{cap} = \frac{\gamma}{\mu}. \tag{6.67}$$

However, in this case the layer must be thick compared to l_{cap}, otherwise surface-tension effects become important, and the fingering transition will change accordingly. This is also a weak constraint since, for most soft materials, we expect l_{cap} to be a few microns. However, with very soft thin layers, the regime with $a \sim l_{cap}$ is surely experimentally accessible, and is likely to be a source of new phenomena.

There remain several outstanding challenges in this area. The first is to prove mathematically that the transition to the fingered state is subcritical. This was shown experimentally and numerically[9,10] but has not yet been treated analytically. Secondly, we speculate that at very small thicknesses surface tension may become important, as it is in the viscous analog associated with Saffman–Taylor fingers; this may modify our purely elastic results. In the analogous Saffman–Taylor fluid problem, surface tension promotes stability, and the same might naively be expected in the elastic case since the formation of large fingers surely increases the interfacial area. However, surface-tension can also drive instability, most famously in the undulating instability of fluid or solid columns,[4,6,7] known as the Rayleigh–Plateau instability. In these cases surface tension drives instability because undulatory perturbations to a cylinder can reduce its area while preserving its volume, so the instability reduces the surface energy. In the elastic fingering case, as the meniscus recedes prior to fingering, it becomes highly curved in the thickness direction, having a shape reminiscent of a half-cylinder. We might similarly expect finger-like undulating perturbations to the meniscus to decrease its area, and hence surface tension to help destabilize the meniscus. Which of these competing intuitions is correct is a promising topic for further work.

Finally, glued joints typically fail *via* stress induced instabilities. Two main categories of failure have been studied: bulk failure of the glue *via* cavitation or fracture, and direct adhesive failure at the meniscus between the glue and the substrate. However, our analysis suggests that stress in a layer of glue under tension tends to be very high at the meniscus of the glue, and that this leads to a fingering instability at the meniscus. Fingering is also a failure mode for elastic seals when they are invaded by the fluid they are intended to contain, generating a leak.[11] We speculate that there is a third category of failure modes for glued joints initiated at the meniscus of the glued layer by elastic fingering. In experiments, the elastic layers are sufficiently compliant to sustain large strains, and while fingering does occur, it often precipitates fracture of the glue and failure of the joint. Elastic fingering is thus a potentially important boundary driven failure mode of glued joints and tight seals. Experimental verification of these failure modes and understanding how to control them would make elastic fingering a problem of some practical importance.

Conflicts of interest

There are no conflicts to declare.

References

1 P. Saffman and G. Taylor, *Proc. R. Soc. London, Ser. A*, 1958, **245**, 312–329.
2 J. L. R. Strutt, *Proc. Lond. Math. Soc.*, 1883, **14**, 170–177.
3 G. Taylor, *Proc. R. Soc. London, Ser. A*, 1950, **201**, 192–196.
4 L. Rayleigh, *Proc. Lond. Math. Soc.*, 1878, **1**, 4–13.
5 S. Mora, T. Phou, J.-M. Fromental and Y. Pomeau, *Phys. Rev. Lett.*, 2014, **113**, 178301.
6 S. Mora, T. Phou, J.-M. Fromental, L. M. Pismen and Y. Pomeau, *Phys. Rev. Lett.*, 2010, **105**, 214301.
7 P. Ciarletta and M. B. Amar, *Soft Matter*, 2012, **8**, 1760–1763.

8 C. Xuan and J. Biggins, *Phys. Rev. E*, 2017, **95**, 053106.
9 B. Saintyves, O. Dauchot and E. Bouchaud, *Phys. Rev. Lett.*, 2013, **111**, 047801.
10 J. S. Biggins, B. Saintyves, Z. Wei, E. Bouchaud and L. Mahadevan, *Proc. Natl. Acad. Sci. U. S. A.*, 2013, **110**, 12545–12548.
11 Q. Liu, Z. Wang, Y. Lou and Z. Suo, *Extreme Mech. Lett.*, 2014, **1**, 54–61.
12 J. Bataille, *Rev. Inst. Fr. Pet.*, 1968, **23**, 1349–1364.
13 J. Nittman, G. Daccord and M. Stanley, *Nature*, 1985, **314**, 391.
14 H. Van Damme, F. Obrecht, P. Levitz, L. Gatineau and C. Laroche, *Nature*, 1986, **320**, 731–733.
15 A. Lindner, D. Bonn, E. C. Poiré, M. B. Amar and J. Meunier, *J. Fluid Mech.*, 2002, **469**, 237–256.
16 S. Wilson, *J. Fluid Mech.*, 1990, **220**, 413–425.
17 H. Zhao and J. Maher, *Phys. Rev. E: Stat. Phys., Plasmas, Fluids, Relat. Interdiscip. Top.*, 1993, **47**, 4278.
18 T. Hirata, *Phys. Rev. E: Stat. Phys., Plasmas, Fluids, Relat. Interdiscip. Top.*, 1998, **57**, 1772.
19 E. Lemaire, P. Levitz, G. Daccord and H. Van Damme, *Phys. Rev. Lett.*, 1991, **67**, 2009.
20 S. Mora and M. Manna, *J. Nonnewton. Fluid Mech.*, 2012, **173**, 30–39.
21 S. Mora and M. Manna, *Phys. Rev. E: Stat., Nonlinear, Soft Matter Phys.*, 2010, **81**, 026305.
22 J. Nase, A. Lindner and C. Creton, *Phys. Rev. Lett.*, 2008, **101**, 074503.
23 M. B. Amar and E. C. Poiré, *Phys. Fluids*, 1999, **11**, 1757–1767.
24 L. Kondic, M. J. Shelley and P. Palffy-Muhoray, *Phys. Rev. Lett.*, 1998, **80**, 1433.
25 P. Coussot, *J. Fluid Mech.*, 1999, **380**, 363–376.
26 A. Lindner, P. Coussot and D. Bonn, *Phys. Rev. Lett.*, 2000, **85**, 314.
27 T. Podgorski, M. C. Sostarecz, S. Zorman and A. Belmonte, *Phys. Rev. E: Stat., Nonlinear, Soft Matter Phys.*, 2007, **76**, 016202.
28 A. He, J. Lowengrub and A. Belmonte, *SIAM J. Appl. Math.*, 2012, **72**, 842–856.
29 G. D. Carvalho, J. A. Miranda and H. Gadêlha, *Phys. Rev. E: Stat., Nonlinear, Soft Matter Phys.*, 2013, **88**, 053006.
30 K. Shull, C. Flanigan and A. Crosby, *Phys. Rev. Lett.*, 2000, **84**, 3057–3060.
31 A. Gent and P. Lindley, *Proc. R. Soc. London, Ser. A*, 1959, **249**, 195–205.
32 S. Lin, T. Cohen, T. Zhang, H. Yuk, R. Abeyaratne and X. Zhao, *Soft Matter*, 2016, **12**, 8899–8906.
33 S. Lin, Y. Mao, H. Yuk and X. Zhao, *Int. J. Solids Struct.*, 2018, **139–140**, 96–104.
34 A. Ghatak and M. K. Chaudhury, *Langmuir*, 2003, **19**, 2621–2631.
35 A. Ghatak, L. Mahadevan, J. Y. Chung, M. K. Chaudhury and V. Shenoy, *Proc. R. Soc. London, Ser. A*, 2004, **460**, 2725–2735.
36 M. Adda-Bedia and L. Mahadevan, *Proc. R. Soc. A*, 2006, **462**, 3233–3251.
37 T. Vilmin, F. Ziebert and E. Raphaël, *Langmuir*, 2010, **26**, 3257–3260.
38 M. K. Chaudhury, A. Chakrabarti and A. Ghatak, *Eur. Phys. J. E: Soft Matter Biol. Phys.*, 2015, **38**, 82.
39 Z. Wei and L. Mahadevan, *Soft Matter*, 2016, **12**, 1778–1782.
40 B. Mukherjee, R. C. Batra and D. A. Dillard, *Int. J. Solids Struct.*, 2017, **110**, 385–403.
41 S. Lin, Y. Mao, R. Radovitzky and X. Zhao, *J. Mech. Phys. Solids*, 2017, **106**, 229–256.
42 J. Biggins, Z. Wei and L. Mahadevan, *Europhys. Lett.*, 2015, **110**, 34001.
43 A. Flamant, *C. R. Acad. Sci., Paris*, 1892, **114**, 1465–1468.
44 M. Levy, *C. R. Acad. Sci., Paris*, 1899, **126**, 1235–1240.